

# Topological Raman Band in Carbon Nanohorn

Ken-ichi Sasaki,\* Yoshiaki Sekine, Kouta Tateno, and Hideki Gotoh

*NTT Basic Research Laboratories, Nippon Telegraph and Telephone Corporation,*

*3-1 Morinosato Wakamiya, Atsugi, Kanagawa 243-0198, Japan*

(Dated: June 23, 2018)

## Abstract

Raman spectroscopy has been used in chemistry and physics to investigate the fundamental process involving light and phonons (quantum of lattice vibration). The carbon nanohorn introduces a new subject to Raman spectroscopy, namely topology. We show theoretically that a photo-excited carrier with a non-zero winding number activates a topological  $D$  Raman band through the Aharonov-Bohm effect. The topology-induced  $D$  Raman band can be distinguished from the ordinary  $D$  Raman band for a graphene edge by its peak position.

Five-membered rings or pentagons are found throughout the honeycomb network of carbon. For example, pentagons appear in a fullerene (buckyball), at the apexes of carbon nanohorns, at the junctions of carbon nanotubes, and in a flat sheet of graphene as a constituent of the Stone-Wales defect.<sup>1-4</sup> A pentagon is a topological defect, which is represented as the flux of a pseudomagnetic field pointing perpendicular to the graphene layer.<sup>5-8</sup> An interesting consequence of such a flux in quantum mechanics is the Aharonov-Bohm (AB) effect. However, the AB effect is usually observed under very silent conditions to maintain coherence, which prevents us from utilizing the AB effect in practical applications. In this letter, we show that a topological defect causes a special band (peak) in the Raman spectrum of a carbon nanohorn, which we call a topological Raman band. A topological Raman band is excited through the AB effect, and can be observed without the need for silent conditions. A photo-excited “relativistic” carrier with a non-zero winding number is the key to activating a topological  $D$  Raman band. The topological  $D$  band consists of zone-boundary  $A_{1g}$  lattice vibration modes, as well as the normal  $D$  band excited near the edge.<sup>9</sup> The phonon modes tend to open an energy gap in the Dirac cone by lifting the degeneracy at the Dirac point (Fig. 1(a)). We will show that a topological  $D$  band is the result of a hybrid between a pentagon and a Dirac point. Note that the Dirac point is a topological defect in the Brillouin zone, and the topological aspect has been highlighted in the absence of a backward scattering mechanism leading to the high mobility of metallic carbon nanotubes.<sup>10</sup>

First, by referring to the Raman process near the armchair edge in Fig. 1(b), we explain that two intervalley scatterings are necessary for the activation of a  $D$  band. The process starts from an electron-hole pair created by an incident laser light. Suppose the electron ( $\bullet$ ) and hole ( $\circ$ ) are located near the K point in the Brillouin zone. When the photo-excited electron emits an  $A_{1g}$  mode, the valley changes from K to K' due to momentum conservation. Meanwhile, the photo-excited hole changes its valley from K to K' as a result of the intervalley scattering at the armchair edge.<sup>11</sup> After the two scattering events, the hole and electron can be annihilated by a scattered light emission. The role of the edge is more clearly understood when we assign different colors to different valleys; red (blue) is used for K (K'). Namely, a change in colors caused by phonon emission must be compensated by intervalley scattering at an armchair edge. In contrast, the color of the trajectory is not altered by pair creation or annihilation because the wavelength of a light is much longer than the wavelength of an electron and hole, and optical transitions are possible only when

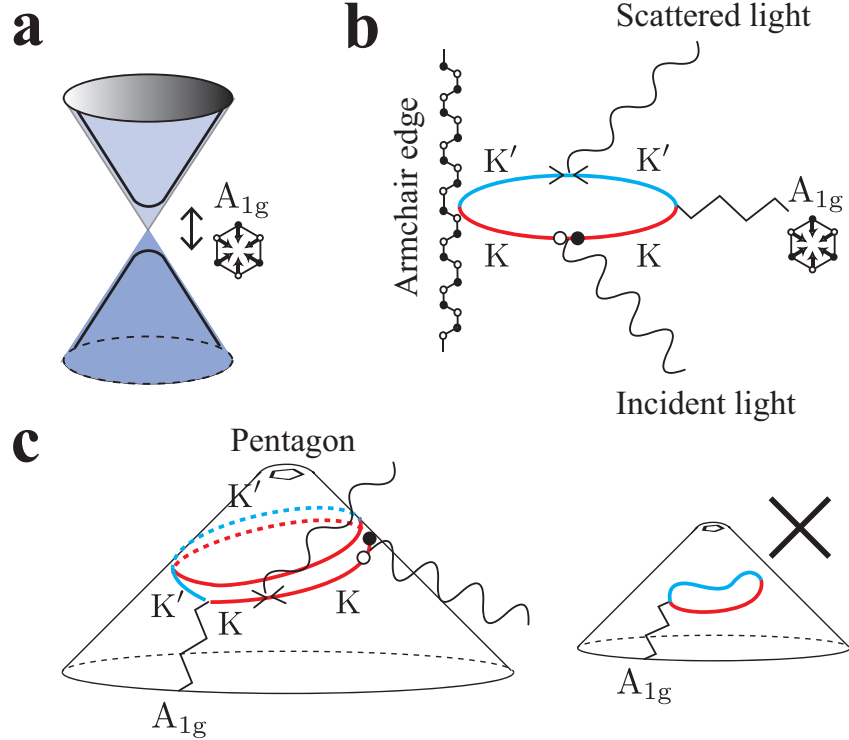


FIG. 1: (a) The zone-boundary  $A_{1g}$  mode is a gap-opening mode. (b) A process exciting the normal  $D$  band at an armchair edge. Two changes in valleys are necessary for the activation of the  $D$  band in the Raman spectrum. (c) A process exciting a topological  $D$  band in a nanohorn. (inset) A trajectory that does not contribute to the  $D$  band in a nanohorn.

the valleys of the electron and hole are the same.

Momentum conservation in a nanohorn allows the activation of a  $D$  band even in the absence of an armchair edge. Figure 1(c) illustrates a typical process that causes a topological  $D$  band in a nanohorn. The characteristic of the trajectory is that it revolves twice around the apex. In contrast, a trajectory that does not turn around the apex (inset in Fig. 1(c)) does not cause a  $D$  band because such a process does not satisfy momentum conservation as regards emitting an  $A_{1g}$  phonon. The difference between the processes in Fig. 1(b) and (c) is the winding number, which is an integer representing the total number of times that a curve travels clockwise around the pentagon. An important point here is that after that the red curve rotates once around the apex, the color changes to blue (i.e., the valley changes automatically) for a topological reason that will be explained below.

A nanohorn can be obtained by first removing the shaded part enclosed by the red and

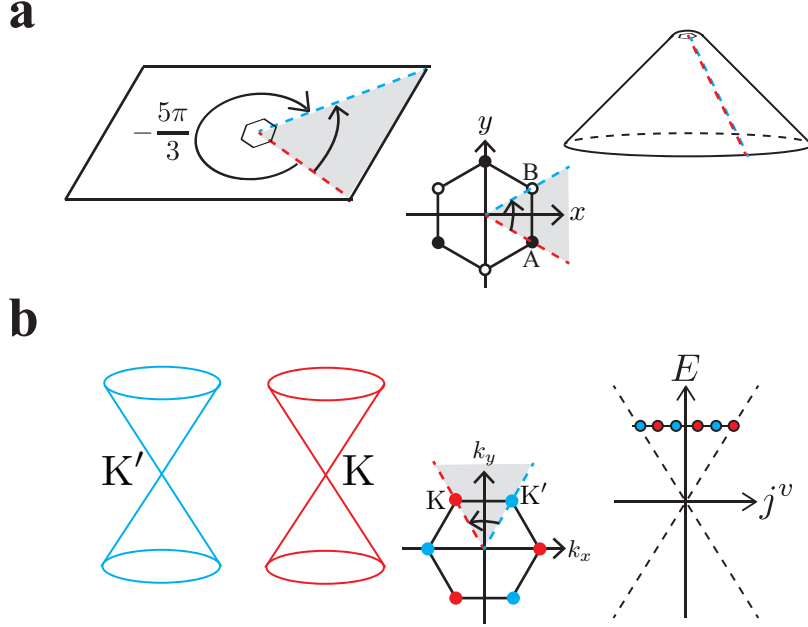


FIG. 2: (a) Sublattice mixing in a nanohorn. A and B atoms are attached so that there is no globally consistent definition of sublattices. (b) Valley mixing in a nanohorn.

blue dashed lines shown in Fig. 2(a) from a flat graphene sheet, and then attaching the red line to the blue line so that the A-atoms (B-atoms) on the red line are identified with the B-atoms (A-atoms) on the blue line. This identification means that it is impossible to make a global distinction between the A and B sublattices in a nanohorn. Furthermore, due to the removal of the part from the graphene layer, the corresponding part is also removed from the Brillouin zone, and the K and K' points are mixed in a nanohorn as shown in Fig. 2(b). Thus, in a nanohorn, it is also impossible to define the K and K' valleys globally. These properties, the lack of a global distinction between A and B atoms, and between K and K' valleys, are unique to a nanohorn and can be traced back to the existence of a pentagon at the apex.

These features of a nanohorn are simply represented by the boundary condition of the wave function:

$$\begin{pmatrix} \psi_A^K(\mathbf{r}') \\ \psi_B^K(\mathbf{r}') \\ \psi_A^{K'}(\mathbf{r}') \\ \psi_B^{K'}(\mathbf{r}') \end{pmatrix} = \begin{pmatrix} 0 & 0 & 0 & -\omega e^{-i\varphi} \\ 0 & 0 & -\bar{\omega} e^{-i\varphi} & 0 \\ 0 & -\bar{\omega} e^{i\varphi} & 0 & 0 \\ -\omega e^{i\varphi} & 0 & 0 & 0 \end{pmatrix} \begin{pmatrix} \psi_A^K(\mathbf{r}) \\ \psi_B^K(\mathbf{r}) \\ \psi_A^{K'}(\mathbf{r}) \\ \psi_B^{K'}(\mathbf{r}) \end{pmatrix}, \quad (1)$$

where  $\mathbf{r}$  is a vector on the surface of a nanohorn,  $\omega \equiv e^{i\frac{\pi}{3}}$ , and the phase  $\varphi$  depends on the position of a pentagon  $\mathbf{R}$  as  $\varphi = 2\mathbf{k}_F \cdot \mathbf{R}$  where  $\mathbf{k}_F = (\frac{4\pi}{3a}, 0)$  is the Fermi wave vector at the K point and  $a$  is a lattice constant.<sup>12</sup> The vector  $\mathbf{r}'$  is the position that is given by the rotation of  $\mathbf{r}$  around the apex:  $\mathbf{r}' = R(-\frac{5\pi}{3})\mathbf{r}$ , where  $R$  denotes a rotation operator around the pentagon. When an electron rotates around  $\mathbf{R}$ , the amplitude of an A-atom at the K valley,  $\psi_A^K(\mathbf{r})$ , changes to that of a B-atom at the K' valley,  $\psi_B^{K'}(\mathbf{r}')$ , with a phase factor  $-\omega e^{i\varphi}$ . The valley and sublattice indexes change topologically through a rotation.

The basis of a wave function that can diagonalize the boundary condition is useful for studying a nanohorn. We apply the following unitary transformation to Eq. (1),

$$\begin{pmatrix} \psi_1(\mathbf{r}) \\ \psi_2(\mathbf{r}) \\ \psi_3(\mathbf{r}) \\ \psi_4(\mathbf{r}) \end{pmatrix} = U^\dagger \begin{pmatrix} \psi_A^K(\mathbf{r}) \\ \psi_B^K(\mathbf{r}) \\ \psi_A^{K'}(\mathbf{r}) \\ \psi_B^{K'}(\mathbf{r}) \end{pmatrix} \equiv \begin{pmatrix} e^{i\varphi} & 0 & 0 & 1 \\ -e^{i\varphi} & 0 & 0 & 1 \\ 0 & e^{i\varphi} & 1 & 0 \\ 0 & -e^{i\varphi} & 1 & 0 \end{pmatrix} \begin{pmatrix} \psi_A^K(\mathbf{r}) \\ \psi_B^K(\mathbf{r}) \\ \psi_A^{K'}(\mathbf{r}) \\ \psi_B^{K'}(\mathbf{r}) \end{pmatrix}, \quad (2)$$

and have

$$\begin{pmatrix} \psi_1(\mathbf{r}') \\ \psi_2(\mathbf{r}') \\ \psi_3(\mathbf{r}') \\ \psi_4(\mathbf{r}') \end{pmatrix} = \begin{pmatrix} -\omega & 0 & 0 & 0 \\ 0 & \omega & 0 & 0 \\ 0 & 0 & -\bar{\omega} & 0 \\ 0 & 0 & 0 & \bar{\omega} \end{pmatrix} \begin{pmatrix} \psi_1(\mathbf{r}) \\ \psi_2(\mathbf{r}) \\ \psi_3(\mathbf{r}) \\ \psi_4(\mathbf{r}) \end{pmatrix}. \quad (3)$$

The Hamiltonian for the original wave function is given by the massless Dirac equation;

$$H_0 = v_F \begin{pmatrix} 0 & \hat{p}_x - i\hat{p}_y & 0 & 0 \\ \hat{p}_x + i\hat{p}_y & 0 & 0 & 0 \\ 0 & 0 & 0 & -\hat{p}_x - i\hat{p}_y \\ 0 & 0 & -\hat{p}_x + i\hat{p}_y & 0 \end{pmatrix}, \quad (4)$$

where  $\hat{p}_i = -i\hbar\partial_i$  denotes a momentum operator and  $v_F$  is the Fermi velocity. The Hamiltonian for the new wave function becomes

$$U^\dagger H_0 U = v_F \begin{pmatrix} 0 & 0 & 0 & -\hat{p}_x + i\hat{p}_y \\ 0 & 0 & -\hat{p}_x + i\hat{p}_y & 0 \\ 0 & -\hat{p}_x - i\hat{p}_y & 0 & 0 \\ -\hat{p}_x - i\hat{p}_y & 0 & 0 & 0 \end{pmatrix}. \quad (5)$$

Here we define the two-component wave functions  $\psi^{v=\pm}$  as

$$\psi^+ \equiv \begin{pmatrix} \psi_2 \\ \psi_3 \end{pmatrix}, \quad \psi^- \equiv \begin{pmatrix} \psi_1 \\ \psi_4 \end{pmatrix}. \quad (6)$$

Using Pauli matrices for sublattices,  $\psi^v$  is expressed as  $\psi^v = -v e^{i\varphi} \sigma_z \psi^K + \sigma_x \psi^{K'}$ . This expression shows that  $v = \pm 1$  originates from the valley degrees of freedom. Since the interaction with the vector potential  $A_i$  of light is given by replacing  $\hat{p}_i$  with  $\hat{p}_i - eA_i$  in Eq. (5), a laser light cannot induce a  $v$ -changing transition.

From Eqs. (3) and (5), the wave functions satisfy the same energy eigen equation

$$E\psi^v(\mathbf{r}) = i\hbar v_F \begin{pmatrix} 0 & \partial_x - i\partial_y \\ \partial_x + i\partial_y & 0 \end{pmatrix} \psi^v(\mathbf{r}), \quad (7)$$

with different boundary conditions,  $\psi^v(\mathbf{r}') = v\sigma_z e^{i\frac{\pi}{3}\sigma_z} \psi^v(\mathbf{r})$ . The solution of the eigenvalue equation was constructed by Lammert and Crespi in a polar coordinate system  $\mathbf{r} \equiv (r, \theta)$  as<sup>6</sup>

$$\psi_{s,k,j^v}^v(r, \theta) = N e^{ij^v\theta} \begin{pmatrix} e^{-i\frac{\theta}{2}} J_{|j^v - \frac{1}{2}|}(kr) \\ -i s e^{i\frac{\theta}{2}} J_{|j^v + \frac{1}{2}|}(kr) \end{pmatrix}, \quad (8)$$

where  $J_\nu$  is a Bessel function with order  $\nu$  and  $N$  is a normalization constant. The solution is characterized by the band index  $s = \pm 1$ , the magnitude of the wave vector  $k$ , and angular momentum  $j^v$ , where the  $j^v$  values are quantized as<sup>6</sup>

$$j^v = (6/5)(n + v/4), \quad (9)$$

where  $n$  is an integer. The energy eigenvalue is  $sE_k$  (where  $E_k = \hbar v_F k$ ), and degeneracy is represented by different  $j^v$  values. Because the normalization of  $r$  ( $0 \leq r \leq R$ ) imposes a constraint  $-kR \lesssim j^v \lesssim kR$ , the density of states increases linearly with increasing energy (See Fig. 2(b)). Although the index  $v$  originates from the valley degrees of freedom, the actual dependence of  $v$  on the wave function appears through the angular momentum  $j^v$ . Namely, the degree of freedom for two valleys is now taken into account by a shift in the angular momentum:  $(5/6)(j^+ - j^-) = 1/2 \pmod{1}$ . Hereafter we write  $\psi_{s,k,j^v}(r, \theta)$  by omitting the superscript from  $\psi_{s,k,j^v}^v(r, \theta)$ .

An  $A_{1g}$  phonon can be excited without changing  $v$ . This is understood by the unitary transformation of the electron-phonon interaction that is derived for a flat graphene sheet

as

$$\begin{aligned}
& U^\dagger \begin{pmatrix} 0 & 0 & 0 & me^{i\mathbf{q}\cdot\mathbf{r}} \\ 0 & 0 & me^{i\mathbf{q}\cdot\mathbf{r}} & 0 \\ 0 & me^{-i\mathbf{q}\cdot\mathbf{r}} & 0 & 0 \\ me^{-i\mathbf{q}\cdot\mathbf{r}} & 0 & 0 & 0 \end{pmatrix} U \\
& = \begin{pmatrix} m \cos(\varphi + \mathbf{q} \cdot \mathbf{r}) & im \sin(\varphi + \mathbf{q} \cdot \mathbf{r}) & 0 & 0 \\ -im \sin(\varphi + \mathbf{q} \cdot \mathbf{r}) & -m \cos(\varphi + \mathbf{q} \cdot \mathbf{r}) & 0 & 0 \\ 0 & 0 & m \cos(\varphi + \mathbf{q} \cdot \mathbf{r}) & im \sin(\varphi + \mathbf{q} \cdot \mathbf{r}) \\ 0 & 0 & -im \sin(\varphi + \mathbf{q} \cdot \mathbf{r}) & -m \cos(\varphi + \mathbf{q} \cdot \mathbf{r}) \end{pmatrix}, \quad (10)
\end{aligned}$$

where  $m$  is an electron-phonon coupling and  $\mathbf{q}$  is the wave vector of an  $A_{1g}$  mode measured from the K point.<sup>13,14</sup> The  $v$ -preserving electron-phonon interactions appear at the diagonal components, which are rewritten as

$$V_{\mathbf{q}}^v = -vm\sigma_z \cos(\varphi + \mathbf{q} \cdot \mathbf{r}), \quad (11)$$

where  $\sigma_z$  results from the fact that an  $A_{1g}$  mode opens an energy gap (Fig. 1(a)). Some  $v$ -changing interactions appear in the off-diagonal components on the right-hand side of Eq. (10), and these do not contribute to a Raman process. Since a  $v$ -changing optical transition cannot be induced by a laser light, a  $v$ -changing scattering by an  $A_{1g}$  mode does not satisfy the momentum selection rule of a Raman process.

The  $\sigma_z$  matrix of  $V_{\mathbf{q}}^v$  plays a decisive role in determining the  $\mathbf{q}$  value. First, let us study the following electron-phonon matrix element,

$$\begin{aligned}
M_{elph}^{(0)} & \equiv \iint \psi_{s,k,j^v}^\dagger(r, \theta) V_{\mathbf{q}}^v \psi_{s,k,j^v}(r, \theta) dS \\
& = -m \iint \psi_{s,k,j^v}^\dagger(r, \theta) \psi_{-s,k,j^v}(r, \theta) \cos(\varphi + qr) dS \\
& \simeq \begin{cases} -\frac{m}{2} \cos(|j^v|\pi + \varphi) & q = 2k \\ 0 & \text{otherwise.} \end{cases} \quad (12)
\end{aligned}$$

Figure 1(c) is the process described by  $M_{elph}^{(0)}$ , which does not include the effect of the existence of a pentagon. Since  $V_{\mathbf{q}}^v$  contains  $\sigma_z$ , an intraband electronic scattering induced by the emission of an  $A_{1g}$  mode is regarded as an interband scattering by a potential  $\cos(\varphi + qr)$ , as shown by the second line. This suggests that  $M_{elph}^{(0)}$  is suppressed in general. The last line

was obtained by using the asymptotic forms for non-negative  $\alpha$ :  $J_\alpha(kr) = \sqrt{2/\pi kr} \cos(kr - \alpha\pi/2 - \pi/4) + \mathcal{O}((kr)^{-1})$ . Although  $M_{elph}^{(0)}$  can be of the order of  $m$  when  $q = 2k$ ,  $M_{elph}^{(0)}$  does not contribute to the  $D$  band because the matrix element depends on  $j^v$ , and so each process experiences a destructive interference in the Raman process, that is,  $\sum_{j^v} \cos(|j^v|\pi + \varphi) \approx 0$ . Next, we calculate the following matrix element:

$$\begin{aligned}
M_{elph}^{(1)} &\equiv \iint \psi_{s,k,j^v}^\dagger(r, \theta) V_{\mathbf{q}}^v \psi_{s,k,j^v}(r, \theta - \frac{5\pi}{3}) dS \\
&= \iint \psi_{s,k,j^v}^\dagger(r, \theta) V_{\mathbf{q}}^v [v\sigma_z e^{i\frac{\pi}{3}\sigma_z}] \psi_{s,k,j^v}(r, \theta) dS \\
&= -m \cos\left(\frac{\pi}{3}\right) \iint \rho_{k,j^v}(r) \cos(\varphi + qr) dS + i \sin\left(\frac{\pi}{3}\right) M_{elph}^{(0)}, \tag{13}
\end{aligned}$$

where  $\rho_{k,j^v}(r) \geq 0$  is the probability density. Figure 1(b) is the process described by  $M_{elph}^{(1)}$ , which takes account of the effect of a non-zero winding number of a photo-excited electron (or hole). When  $q = 0$ , the first term leads to  $-\frac{m}{2} \cos(\varphi)$  due to normalization  $\iint \rho_{k,j^v}(r) dS = 1$ . When  $q \neq 0$ , the first term is suppressed by the integral about  $r$ . The first term is independent of  $j^v$ , which is in contrast to  $M_{elph}^{(0)}$ . For a general case, we define  $M_{elph}^{(w)} \equiv \iint \psi_{s,k,j^v}^\dagger(r, \theta) V_{\mathbf{q}}^v \psi_{s,k,j^v}(r, \theta - \frac{5\pi}{3}w) dS$ , and obtain

$$\frac{\sum_{j^v} M_{elph}^{(w)}}{\sum_{j^v}} = \begin{cases} -ivm \sin\left(\frac{\pi}{3}w\right) \cos(\varphi) & w = \text{even}, \\ -m \cos\left(\frac{\pi}{3}w\right) \cos(\varphi) & w = \text{odd}, \end{cases} \tag{14}$$

where we assume  $q = 0$ . Similarly, the optical matrix element is given by

$$M_{opt}^{(w)}(s) = \begin{cases} -ev_F A_r \frac{is\pi}{2R} \cos\left(\frac{\pi}{3}w\right) & w = \text{even}, \\ ev_F A_r \frac{vs\pi}{2R} \sin\left(\frac{\pi}{3}w\right) & w = \text{odd}. \end{cases} \tag{15}$$

Here  $A_r$  is the vector potential for a circularly polarized light.

The probability amplitude for a Raman process that can contribute to a topological  $D$  band in a nanohorn is written as

$$M_\varepsilon^{(l,m,n)} = \int dS^3 \text{Tr} \left[ G_{\varepsilon-E_L}^{(l)}(r, \theta; r'', \theta'') \hat{H}_{sc} G_{\varepsilon-\hbar\omega}^{(m)}(r'', \theta''; r', \theta') V_{\mathbf{q}} G_\varepsilon^{(n)}(r', \theta'; r, \theta) \hat{H}_{in} \right], \tag{16}$$

where  $E_L$  and  $\hbar\omega$  are laser energy and phonon energy, respectively. Here,  $G_\varepsilon^{(w)}(r', \theta'; r, \theta)$  is the probability amplitude that an electron at  $(r, \theta)$  with energy  $\varepsilon$  propagates in a nanohorn



and arrives at  $(r', \theta')$  after rotating  $w$  times around the apex in a clockwise direction. Explicitly, it is written as

$$G_\varepsilon^{(w)}(r', \theta'; r, \theta) = \sum_{s,k,j^v} \frac{[v\sigma_z e^{i\frac{\pi}{3}\sigma_z}]^w \psi_{s,k,j^v}(r', \theta') \psi_{s,k,j^v}^\dagger(r, \theta)}{\varepsilon - sE_k + i\gamma}, \quad (17)$$

where  $\hbar/\gamma$  is the mean lifetime of an electron. It is reasonable to assume that a higher winding number does not contribute to the Raman process because an electron (or hole) experiences scattering caused by impurities and defects, and so  $G_\varepsilon^{(w)}$  is suppressed. Thus, we focus on the most important process contributing to the  $D$  band, that is, the process shown in Fig. 1(b):

$$M_\varepsilon^{(0,0,1)} = \text{Tr} \left[ \sum_{s,k,j^v} \frac{M_{opt}^{(0)}(-s) M_{elph}^{(1)} M_{opt}^{(0)}(s)}{(\varepsilon - E_L + sE_k + i\gamma)(\varepsilon - \hbar\omega - sE_k + i\gamma)(\varepsilon - sE_k + i\gamma)} \right]. \quad (18)$$

When  $\gamma \ll \varepsilon_R$  ( $\equiv E_L/2$ ), a resonance process dominates other off-resonant processes, and we obtain

$$M_{\varepsilon_R}^{(0,0,1)} \propto \frac{\pi}{\hbar\omega - 2i\gamma} \left\{ \frac{\varepsilon_R}{\gamma} \left( 1 - i \frac{\gamma}{\hbar\omega} \right) - i \right\} |M_{opt}^{(0)}|^2 M_{elph}^{(1)}. \quad (19)$$

It is noteworthy that the Raman process is represented as a first-order Raman process, i.e., a photo-excited electron is scattered only once, which is the same as the  $G$  Raman band in flat graphene.<sup>14,15</sup>

The topological  $D$  band is distinguished from the normal  $D$  band induced by the edge of a nanohorn by the peak position in the Raman spectrum, because the self-energy of the  $A_{1g}$  mode increases linearly with increasing  $q$ .<sup>14,16</sup> The wave vector of an  $A_{1g}$  mode with a topological origin is  $q \simeq 0$ , while that of the normal  $A_{1g}$  mode is  $q \simeq 2k$  (where  $2k$  is proportional to  $E_L/\hbar v_F$ ). Thus, a topological  $D$  peak appears on the low-energy side of the peak position of the normal  $D$  peak, and we estimate the shift to be approximately  $50 \text{ cm}^{-1}$  when  $E_L = 1.6 \text{ eV}$  (wavelength is  $750 \text{ nm}$ ).<sup>14,16</sup> The shift increases almost linearly with increasing the  $E_L$  value (see Fig.3(c) in Ref. 16 for details) because of the non-dispersive (dispersive) behavior of the topological (normal)  $D$  peak. The abnormal  $q$  value (null  $q$ ) means that an  $A_{1g}$  phonon is created by the forward scattering of a photo-excited electron. This is in contrast to the fact that an  $A_{1g}$  phonon with  $q \simeq 2k$  is a consequence of the backward scattering of a photo-excited electron near the armchair edge.<sup>14</sup> The forward scattering results from the identification of A and B atoms, which is enforced through a rotation about the pentagon and is not seen at the armchair edge.

The region in which a topological  $D$  band can be activated, is limited to near the pentagon. This is because, the period of a rotation for an electronic state that is distant from the pentagon is longer than that for a state near the pentagon, and a state with a long rotational period is subject to a strong dephasing effect. Note that the analysis using the wave function of Eq. (8) is valid when the mean lifetime of electron  $\tau$  is longer than the period of a rotation,  $\tau_c \equiv 5\pi r/3v_F$ . For example, when  $\tau = 200$  fs,  $r < 40$  nm. There are some perturbations that can shorten  $\tau$  or  $r$ , in addition to the  $\nu$ -changing part in the electron-phonon interactions of an  $A_{1g}$  mode. For example, it can be shown that the electron-phonon interactions for optical and acoustic phonons near the  $\Gamma$  point and the hybridization between  $\sigma$  and  $\pi$  orbitals caused by the curvature at the apex of a nanohorn are categorized by  $\nu$ -changing perturbations. This also means that the  $G$  band is suppressed where the topological  $D$  band is enhanced.

A pentagon is not a unique topological defect in a graphene layer. A heptagon also serves as a topological defect, for which we can derive the same conclusion as that obtained for a pentagon. Namely, a topological  $D$  band is induced by paths such as 1 and 2 shown in Fig. 3. There is a pentagon-heptagon pair at the junctions of carbon nanotubes.<sup>2</sup> The trajectories traveling around a pair do not contribute to a topological  $D$  Raman band (paths 3 and 4 in Fig. 3) by cancellation. In fact, a pentagon (heptagon) is regarded as the flux  $v\Phi_0/4$  ( $-v\Phi_0/4$ ),<sup>6</sup> and the AB effect is suppressed for paths 3 and 4. We speculate that a topological  $D$  band does not vanish unless the distance between the pentagon and heptagon is of the order of the bond length. This condition would be satisfied for nanohorns and the junctions of carbon nanotubes, but not for Stone-Wales defects.

In conclusion, a pentagon allows a topological  $D$  band to appear in the Raman spectrum of a nanohorn. A topological Raman band is the result of the AB effect in Raman spectroscopy, and a non-zero winding number of the trajectory of a photo-excited electron (or hole) is the key factor as regards enhancing the intensity. The peak position of a topological  $D$  band differs by about  $50 \text{ cm}^{-1}$  from that of the normal  $D$  band activated at the edge. This difference arises due to the lack of a global distinction between A and B atoms in a nanohorn.

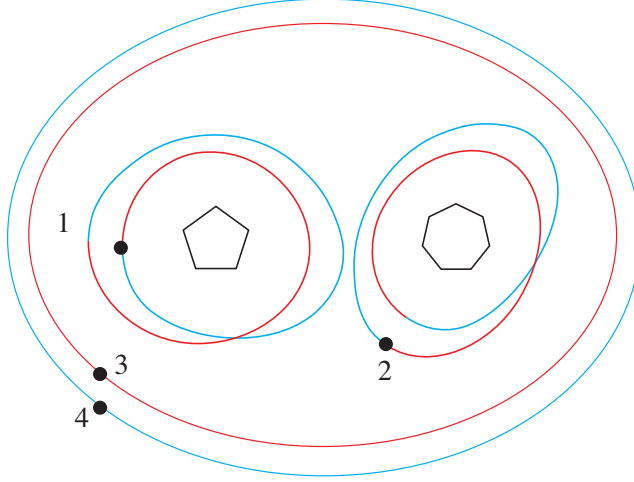


FIG. 3: Paths 1 and 2 are trajectories that are able to activate a topological  $D$  band. Paths 3 and 4 that travel around a pentagon-hexagon pair do not contribute to the  $D$  band.

### Acknowledgments

We are grateful to Yasuhiro Tokura for helpful discussions.

- 
- \* Electronic address: sasaki.kenichi@lab.ntt.co.jp
- <sup>1</sup> H. W. Kroto, J. R. Heath, S. C. O'Brien, R. F. Curl, and R. E. Smalley, *Nature* **318**, 162 (1985).
- <sup>2</sup> S. Iijima, T. Ichihashi, and Y. Ando, *Nature* **356**, 776 (1992).
- <sup>3</sup> S. Iijima, M. Yudasaka, R. Yamada, S. Bandow, K. Suenaga, F. Kokai, and K. Takahashi, *Chem. Phys. Lett.* **309**, 165 (1999).
- <sup>4</sup> A. Hashimoto, K. Suenaga, A. Gloter, K. Urita, and S. Iijima, *Nature* **430**, 870 (2004).
- <sup>5</sup> J. González, F. Guinea, and M. A. H. Vozmediano, *Phys. Rev. Lett.* **69**, 172 (1992).
- <sup>6</sup> P. E. Lammert and V. H. Crespi, *Phys. Rev. Lett.* **85**, 5190 (2000).
- <sup>7</sup> K. Sasaki, Y. Kawazoe, and R. Saito, *Prog. Theor. Phys.* **113**, 463 (2005).
- <sup>8</sup> R. Jackiw and S.-Y. Pi, *Phys. Rev. Lett.* **98**, 266402 (2007).
- <sup>9</sup> F. Tuinstra and J. L. Koenig, *J. Chem. Phys.* **53**, 1126 (1970).
- <sup>10</sup> T. Ando, T. Nakanishi, and R. Saito, *J. Phys. Soc. Jpn.* **67**, 2857 (1998).
- <sup>11</sup> L. G. Cançado, M. A. Pimenta, B. R. A. Neves, M. S. S. Dantas, and A. Jorio, *Phys. Rev. Lett.*

**93**, 247401 (2004).

<sup>12</sup> H. Matsumura and T. Ando, J. Phys. Soc. Jpn. **67**, 3542 (1998).

<sup>13</sup> K. Sasaki and R. Saito, Prog. Theor. Phys. Suppl. **176**, 253 (2008).

<sup>14</sup> K.-i. Sasaki, Y. Tokura, and T. Sogawa, Crystals **3**, 120 (2013).

<sup>15</sup> K.-i. Sasaki, K. Kato, Y. Tokura, S. Suzuki, and T. Sogawa, Phys. Rev. B **85**, 075437 (2012).

<sup>16</sup> K.-i. Sasaki, K. Kato, Y. Tokura, S. Suzuki, and T. Sogawa, Phys. Rev. B **86**, 201403 (2012).